JTTEE5 8:301-314

Flattening of Droplets and Formation of Splats in Thermal Spraying: A Review of Recent Work—Part 2

V.V. Sobolev and J.M. Guilemany

(Submitted 3 May 1998; in revised form 2 September 1998)

This is the second part of a review article that deals with an analysis of the influence of wetting at the substrate-coating interface and surface phenomena, substrate deformation, dynamics of splashing, splat-substrate interaction and spraying at off-normal angles on droplet flattening, and the formation of splats in thermal spraying, which affects the coating quality. The results agree well with experimental data and improve understanding of the thermal spray processes to make them more effective.

Keywords off-normal spraying, review, splat formation, wetting behavior

1. Introduction

This article is the second part of a review dedicated to the droplet flattening and the splat formation in thermal spraying. It follows Part 1 (Ref 1) and covers the following issues that produce a noticeable effect on the flattening process:

- Wetting and surface phenomena
- Substrate deformation
- Splashing of the impinging droplets
- Splat-substrate interaction
- Spraying at off-normal angles

These factors are important in order to understand coating formation during thermal spraying and increase quality of coatings produced for different industrial applications.

2. Effect of Wetting and Surface Phenomena

It is well known that the main part of droplet kinetic energy is transformed into the energy of viscous forces (Ref 2-4). In the mechanics of droplet spreading, the surface forces play an important role at the end of the flattening process because they stop the flattening and determine a characteristic time of the process (Ref 3). Wetting between the spreading droplet and the substrate plays an important role in the droplet flattening because it affects not only the surface phenomena but also the contact thermal resistance at the splat-substrate interface, which is an important parameter for the development of the coating structure (Ref 5). This section involves an analysis of the influence of wetting and the surface effects on the parameters of droplet flattening and splat formation. Special attention is given to the effect of wetting on the development of porosity.

V.V. Sobolev and **J.M. Guilemany,** CPT Thermal Spray Centre, Materials Engineering Department, Enginyería Química i Metallúrgia, Universitat de Barcelona, Marti i Frangués, 1. E-08028 Barcelona, Spain. Contact e-mail: sobolev@angel.qui.ub.es.

2.1 Influence of Wetting on Droplet Flattening

The formulas for splat thickness and radius in Section 2 of Part 1 (Ref 1) were obtained under an assumption that the main part of the droplet kinetic energy is used to overcome the viscous forces at the substrate surface (Ref 2, 3). This assumption is valid when the Weber number, $We = \rho U^2 R_p \sigma^{-1}$ (where ρ is the density of the droplet, U is the velocity of the droplet impingement, R_p is the droplet radius, and σ is the surface tension coefficient), exceeds the Reynolds number, $Re = 2R_p U \rho \mu^{-1}$ (where μ is the dynamic viscosity of the droplet material). That is, $We >> Re^{1/2}$ (Ref 3). This situation is typical for thermal spraying.

Wetting has an important influence on the development of the contact between the lower surface of the splat and the substrate surface (Ref 6). Thus, it affects the value of the contact heat transfer coefficient, α_c, which determines the rate of the heat transfer from the splat to the substrate (Ref 5). Taking into

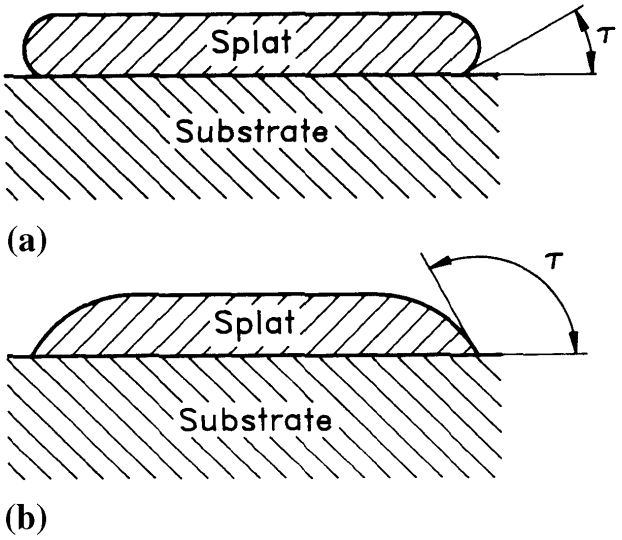

Fig. 1 Wetting angles between liquid splat and substrate

account that the value of α_c increases with a decrease in the contact wetting angle, τ, between the substrate and the flattening droplet, Fig. 1, it is possible to introduce an effective value, α_{c*}, of the heat transfer coefficient α_c:

$$\alpha_{c*} = 0.5\alpha_c(1 + \cos\tau) \quad \text{(Eq 1)}$$

In the case of ideal wetting when $\tau = 0$, it is obtained from Eq 1 that $\alpha_{c*} = \alpha_c$. When the angle τ increases and wetting worsens, then the contact between the splat and the substrate is also adversely affected, and the value of α_{c*} decreases. This leads to a decrease in the velocity of the splat solidification, V_{s*}, which depends on the value of α_{c*} and can be presented in a form:

$$V_{s*} = \alpha_{c*}T_p/(q_p\rho) \quad \text{(Eq 2)}$$

where T_p is the droplet temperature and q_p is the latent heat of fusion of the droplet material.

Thus the solidification velocity, V_{s*}, in Eq 2 decreases with an increase in τ. To take wetting into account, it is necessary to

Nomenclature

a	thermal diffusivity, m^2/s
A_1	Parameter in Eq 6
b	Splat thickness, m
B_1	Parameter in Eq 6
c	Sound velocity, m/s
c_1	Specific heat, J/kgK
D	Splat diameter, m
E	Dimensionless parameter in Eq 38
F	$F = U\exp(UR_p^{-1}t)$
G	Thermal gradient, K/m
K	Semiempirical coefficient in Eq 28, m/sK^2
P	Pressure, N/m^2
P_a	Average pressure, N/m^2
P_g	Gas pressure, N/m^2
P_{im}	Impact pressure, N/m^2
P_σ	Capillary pressure, N/m^2
q	Heat flux, W/m^2
q_p	Latent heat of fusion of the droplet material, J/kg
Q_1	Released heat, J
Q_2	Heat spent for heating, J
r	Radial coordinate, m
r_k	Critical radius of embryo of crystallization, m
R	Splat radius, m
R_c	Contact thermal resistance, m^2K/W
R_P	Particle radius, cavity radius, m
R_{pr}	Pore radius, m
Re	Reynolds number: $Re = 2R_pU\rho/\mu$
t	Time, s
t_f	Characteristic time of completion of flattening, s
t_{fr}	Characteristic time of completion of flattening due to surface roughness, s
t_{fs}	Characteristic time of completion of flattening due to surface effects, s
$t_{0.9}$	Characteristic time of 90% completion of flattening, s
T	Splat temperature, °C
T_k	Melting point of droplet material, °C
T_{oh}	Splat initial overheating, °C
T_s	Substrate temperature, °C
T_{sb}	Substrate temperature at the splat-substrate interface, °C
T_{sp}	Splat temperature at the splat-substrate interface, °C
T_{tr}	Transition temperature, °C
U	Particle (droplet) impact velocity, ms^{-1}
$\|U\|$	Absolute value of U, m/s
U_n	Normal component of U, m/s
V_c	Cooling velocity, K/s
V_s	Solidification velocity, m/s
We	Weber number: $We = \rho U^2R_p/\sigma$
Y	Dimensionless parameter: $Y = P_m/P_{im}$

Greek Symbols

α	Dimensionless parameter: $\alpha = \varepsilon/R_p$
β	Dimensionless parameter: $\beta = V_s/U$
γ	$\gamma = \exp(0.4\theta)$
γ_1	Empirical coefficient
δ	Thickness of splat lower part, m
ΔP	Increment of pressure, N/m^2
ΔT	Supercooling, °C
ΔT_h	Thermal super-cooling, °C
ΔT_p	Super-cooling developed by pressure, °C
ε	Roughness size, m
ζ	Dimensionless splat thickness: $\zeta = b/R_P$ and pressure ratio: $\zeta = P_a/P_m$
η	$\eta = r/R$
θ	Dimensionless time: $\theta = U R_p^{-1}t$
ι	Substrate curvature, m^{-1}
μ	Droplet dynamic viscosity, Ns/m^2
ξ	Dimensionless splat radius: $\xi = R/R_P$
ρ	Droplet density, kg/m^3
σ	Coefficient of surface tension, N/m
τ	Wetting angle, (degree)
υ	Specific heat ratio
φ	Spraying angle, (degree)
χ	Dimensionless parameter of droplet mass loss
ψ_1	Dimensionless parameter
ψ_2	Dimensionless parameter
ψ_3	Dimensionless parameter
ψ_o	Function of φ in Eq 31, 32

Subscripts

c	Critical
e	Effective
f	Final
m	Maximum
o	Initial
p	Particle
*	Characteristic

substitute the value of V_s in the formula for the final values of the splat thickness, $\zeta_f = b/R_p$, and radius, $\xi_f = R/R_f$, by the value of V_{s*} from Eq 2. Thus, an increase in the contact wetting angle causes an increase in the splat thickness and a decrease in the splat radius. It also follows that the influence of wetting on the flattening process decreases with an increase in the velocity, U, of the droplet impingement onto the substrate surface, which leads to a decrease in the parameter, $\beta_* = V_{s*}U^{-1}$. At the same time, an increase in the substrate initial temperature, T_{so}, gives rise to the solidification velocity, V_{s*}, and contributes to an increase in the effect of wetting on the droplet flattening. Thus, an increase in T_{so} gives rise to an effect that is similar to a decrease in the contact wetting angle.

The final values of the dimensionless splat thickness, $\zeta_f = b/R_p$, and radius, $\xi_f = R/R_p$ (where b and R are the splat thickness and radius, respectively), have a form:

$$\zeta_f = 1.826\, Re^{-1/2}[1 + 0.12(\alpha\, Re)^{1/2} - 0.68\beta_*\, Re^{1/2} \ln(0.3\, Re)]$$

$$\alpha = \varepsilon/R_p \qquad \text{(Eq 3)}$$

$$\xi_f = 0.8546\chi^{1/2}\, Re^{1/4}[1 - 0.06(\alpha\, Re)^{1/2} + 0.34\beta_*\, Re^{1/2} \ln(0.3\, Re)] \qquad \text{(Eq 4)}$$

where ε is the height of the roughness "teeth" on the substrate surface. Figure 2 shows that an increase in the contact wetting angle leads to an increase in the final splat thickness and to a decrease in the final splat radius.

The splat can contain dissolved oxygen due to diffusion in the liquid phase of the droplet and the splat during thermal spraying (Ref 7). The presence of dissolved oxygen is established to cause a decrease in the contact wetting angle and an improvement of wetting between the substrate and the liquid splat (Ref 8).

2.2 *Influence of Wetting on the Development of Porosity*

Gas and shrinkage porosity are often formed in thermally sprayed coatings (Ref 9-12). The most important is gas porosity, which is usually detrimental to coating properties. To decrease porosity it is necessary to improve understanding of the factors that have a prime influence on this process. Wetting is among these factors. Consider flattening of the droplet on the rough substrate when there is a good (τ = <90°) and poor (τ = > 90°) wetting between the liquid splat and the substrate (Fig. 3). In this case a gas cavity is formed between the "teeth" of the surface profile and the liquid splat. When τ = <90° (Fig. 3a), consider an equilibrium condition where the sum of the pressure developed in the flattening splat, P, and the capillary pressure, P_σ, is equal to the gas pressure, P_g, inside the cavity (Ref 11-15):

$$P + P_\sigma = P_g \qquad P_\sigma = 2\sigma\cos\tau/R \qquad P_g = P_{go}(R_o/R)^{3\upsilon} \qquad \text{(Eq 5)}$$

where R_o and R are the initial and current values of the cavity radius, P_{go} is an initial value of the gas pressure, and υ is the specific heat ratio. Consider for simplicity an isothermal case when υ = 1. Then from Eq 5 the cubic equation for the cavity radius, R, is transformed to:

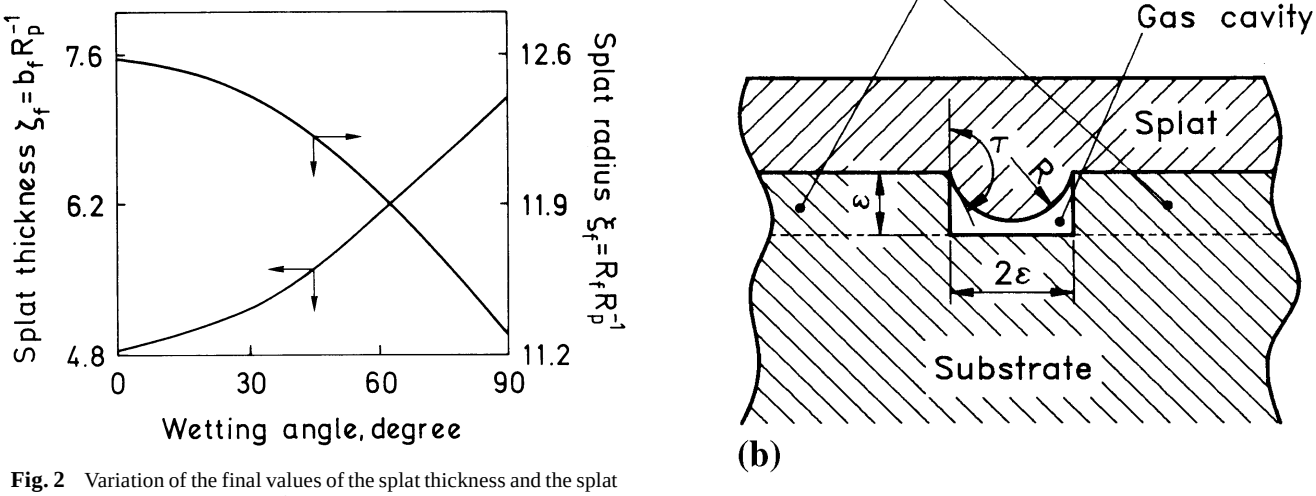

Fig. 2 Variation of the final values of the splat thickness and the splat radius with a wetting angle (Ref 6)

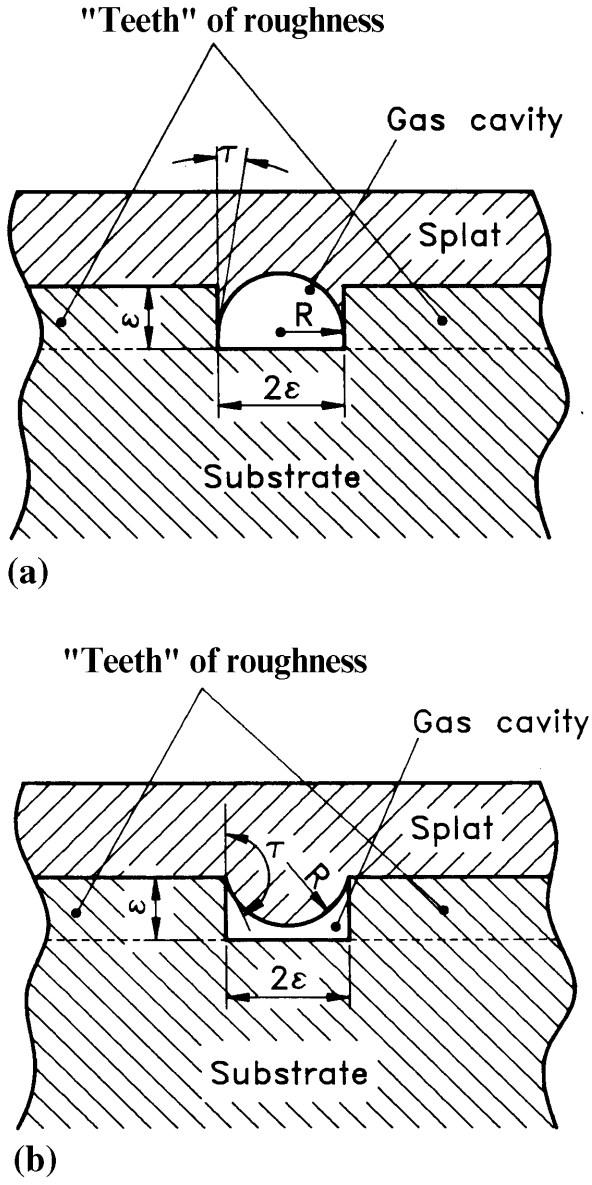

Fig. 3 Influence of wetting on formation of pores in splat

$$R = 2^{1/3}B_1^{1/3}R_o\,[1 - 2A_1^3/(81B_1)] \quad A_1 = 2\sigma\cos\tau/(PR_o)$$

$$B_1 = P_{go}/P \qquad \text{(Eq 6)}$$

In the case of poor wetting when $\tau = >90°$ (Fig. 3b), the formula for the cavity radius is similar to Eq 6. From Eq 6 it is seen that the cavity radius decreases with an increase in σ and a decrease in τ. The cavity radius is minimum when $\tau = 0$. After solidification this cavity is transformed into a pore. Because the velocity of the splat solidification is much greater than the velocity of diffusion of the dissolved gases from the liquid splat to the cavity, the value of R can be considered as the pore radius, which is developed after solidification. Thus, under the same spray conditions the splat porosity increases with an increase in the contact wetting angle, that is, when wetting between the splat and substrate is poor.

2.3 Effect of the Surface Phenomena on Flattening

The main part of the droplet kinetic energy is dissipated upon impact and transformed into the energy of the viscous forces (Ref 2-4, 13). The surface processes start to play a role when the droplet kinetic energy essentially decreases. This occurs at the final stage of flattening. The influence of the surface phenomena on the droplet flattening was studied in Ref 3, 4.

In Ref 4, an analytical correlation between the final value of the dimensionless splat radius, ξ_f, and the Weber number, *We*, and the Reynolds number, *Re*, was established. In the special case of very high Reynolds numbers the variation of ξ_f was shown to be dependent only on the Weber number: $\xi_f = (We/3)^{1/2}$, provided that $We = > 100$. These values of *We* correspond to thermal spray applications.

Modeling of the droplet flattening undertaken in Ref 3 shows that the surface tension has no practical influence in the early stages of the process. Later, when the surface tension forces overcome those of inertia, a liquid film breakup in the spreading process occur. The breakup will occur later with an increase in the droplet impact velocity.

Thus, the surface forces arrest the flattening process. It is worth estimating the characteristic time of this event. The pressure, P, developed upon the droplet impact promotes spreading of the liquid on the substrate surface. Flattening stops when P becomes equal to the capillary pressure, $P_{sf} = 2\sigma\cos\tau b^{-1}$, which hinders the spreading process (Ref 6). It is important to know the time, t_f, of finishing the droplet flattening. Assuming $P = P_{sf}$, $\alpha = 0$, and $\beta = 0$, (Ref 6):

$$t_f = 2.5a^{-1}\ln(0.144\chi^{1/2}We) \qquad a = UR_p^{-1} \qquad \text{(Eq 7)}$$

It is interesting to compare this time with the time, $t_{0.9}$, which is the time required to reach 90% completion of flattening. The analytical expression for $t_{0.9}$ is obtained in Ref 13 and 14 under an assumption that the major part of the droplet kinetic energy is dissipated during flattening due to the viscous effects. When *Re* $> > 1$, from Ref 13, 16, it is found that

$$t_{0.9} = 1.125a^{-1}\ln(0.3\,Re) \qquad \text{(Eq 8)}$$

The ratio, ψ_1, of the time, $t_{0.9}$, to t_f is:

$$\psi_1 = 0.45\ln(0.3\,Re)/\ln(0.144\chi^{1/2}We) \qquad \text{(Eq 9)}$$

Consider, for example, plasma spraying of molybdenum powder particles when $R_p = 20$ μm, $\rho = 9900$ kgm^{-3}, $U = 150$ ms^{-1}, $\sigma = 1$ Nm^{-2}, $\mu = 0.003$ kg (ms)$^{-1}$, and $\chi = 0.8$, then *Re* = 30,000, *We* = 4455, and $\psi_1 = 0.62$. Thus, the characteristic time, $t_{0.9}$, is markedly less than the value of t_f. The flattening process may be hindered by the surface roughness (Ref 14). Using the results obtained in Ref 14 and 17, it can be shown that the finishing time, t_{fr}, for the splat flattening due to the surface roughness is:

$$t_{fr} = 2.5a^{-1}\ln[(1 + 10\alpha^{-1/2})/3] \qquad \text{(Eq 10)}$$

The ratio, ψ_2, of the time, t_{fr}, to $t_{0.9}$ can be written:

$$\psi_2 = 2.22\ln[(1 + 10\alpha^{-1/2})/3]\ln(0.3\,Re) \qquad \text{(Eq 11)}$$

When *Re* = 30,000 and $\alpha = 0.1$, then $\psi_2 = 0.85$. Therefore, due to dissipation of the droplet kinetic energy caused by the roughness, the flattening process was completed earlier than in the case where the roughness was absent. In the presence of roughness, the splat thickness increases in comparison with the case when $\alpha = 0$ and, hence, the capillary pressure, P_σ, decreases and the surface effects start to break the flattening process later. The time for the flattening to finish, t_{fs}, in this case is:

$$t_{fs} = 2.5a^{-1}\ln(0.144\,We\,\chi^{-1/2} + 0.016\,We^2\,\alpha^{1/2}\chi^{-1}) \qquad \text{(Eq 12)}$$

Solidification of the lower part of the splat during flattening leads to a decrease in the splat thickness (Ref 17, 18) and to an increase in P_{sf}. Thus, the time of finishing of the flattening process, t_{fl}, decreases. For a smooth surface, t_{fl}, can be shown to have a form:

$$t_{fl} = t_f(1 + 1.27\beta\,We)^{-1} \qquad \text{(Eq 13)}$$

When $\alpha = 0$ and $\beta = 0$, the final values of the dimensionless splat thickness, ζ_f, and the splat radius, ξ_f, can be written as:

$$\zeta_f = 6.93\chi^{1/2}\,We^{-1} \qquad \text{(Eq 14)}$$

$$\xi_f = 0.439\chi^{1/4}\,We^{1/2} \qquad \text{(Eq 15)}$$

The splat radius is seen to increase with decreasing surface tension. This agrees with the modeling results presented in Ref 3. The formula from Eq 15 for ξ_f is slightly different from that found by others (e.g., $\xi_f = 0.577\,We^{1/2}$ in Ref 4). For example, in the case of the plasma spraying of molybdenum powder particles with the previously mentioned spray parameters, it is obtained from Eq 14 and 15 that $b_f = 0.03$ μm and $R_f = 554$ μm.

It must be taken into account that even if the substrate surface is considered to be smooth its roughness can be approximately 0.1 to 1 μm, which exceeds the estimated value of the final splat thickness, b_f. As a result the flattening process becomes unstable, splashing occurs, the splat loses its regular shape, and splash-shaped splats are formed. Splashing can be avoided by increasing the substrate initial temperature (Ref 19, 20). But this refers mainly to the substrate surface with a very small roughness.

Thus, it seems that in practice the formulas in Eq 14 and 15 describing variations of the final splat thickness and the final splat radius with the Weber number when the surface effects dominate (as well as the similar formula found by others) (Ref 3, 4), cannot be used to estimate the values of b_f and R_f in thermal spraying. For these purposes, the equations for b_f and R_f, depending on the Reynolds number (when the viscous effects play the major role), must be used (Ref 2, 16, 17, 21, 22). The same applies to Eq 12 and 13, which estimate the values of t_{fs} and t_{fl}. The flattening process is believed to be finished before influences due to roughness and solidification on the surface effects take effect.

3. Influence of Substrate Deformation

Assume that droplet impact causes the substrate to have curvature, ι, and the substrate becomes concave (positive curvature) or convex (negative curvature) in the direction of the droplet impingement (Fig. 4). Assume that the curvature is positive. Then the following equations describing the droplet flattening characteristics for the typical thermal spray situation when $Re >> 1$ are obtained (Ref 23).

$$\zeta = \gamma^{-1}(1 + 0.8\iota\, Re\, \theta^2)^{1/2} \qquad \gamma = \exp(0.4\theta) \qquad \text{(Eq 16)}$$

$$\xi = 1.155(\chi\gamma)^{1/2}(1 + 0.8\iota\, Re\, \theta^2)^{-1/4} \qquad \text{(Eq 17)}$$

When $\iota = 0$ from Eq 16 and 17, the formula established in Ref 17 comes. When the curvature is negative, the corresponding terms in Eq 16 and 17 change the signs. It can be seen that the substrate negative curvature ($\iota < 0$) leads to a decrease in the splat thickness and an increase in the splat radius in comparison with the case of a flat substrate ($\iota = 0$). Positive curvature ($\iota > 0$) contributes to an increase in the splat thickness and to a decrease in the splat radius during flattening. Thus, the influence of the positive substrate curvature is similar to that of the substrate roughness, which hinders droplet spreading in flattening (Ref 14, 21). Typical variations of ζ and ξ with increasing θ are shown in Fig. 5 and 6 for the different values of ι.

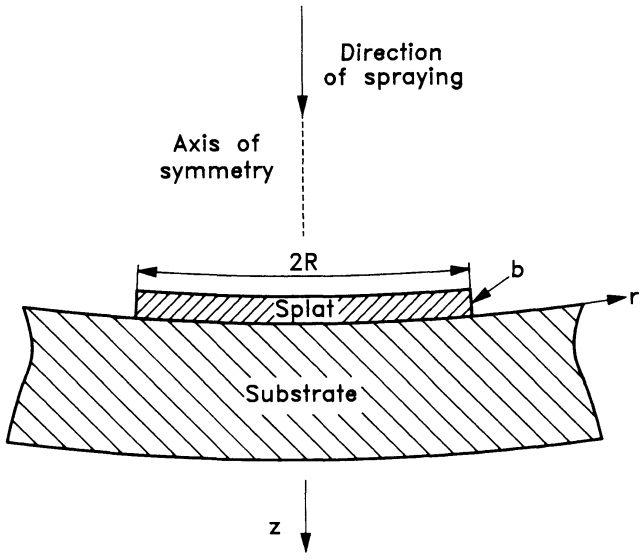

Fig. 4 Substrate deformation during splat formation

Next the time of finishing of the flattening process when $\iota > 0$ will be established. This process finishes when $d\zeta/d\theta = 0$ and $d\xi/d\theta = 0$. From the results of Ref 23 it follows that this occurs at the time $\theta = \theta_f$:$\theta_f = 0.5\ (\iota\, Re)^{-1}$. It is interesting to compare this time with the time $\theta_{0.9}$, which is defined as a time required to reach 90% completion of flattening (Eq 8). The ratio ψ_3 of θ_f to $\theta_{0.9}$ has the following form: $\psi_3 = \theta_f/\theta_{0.9} = 0.444\ [\iota\, Re \ln(0.3\, Re)]^{-1}$.

Parameter ψ_3 decreases with increasing ι and *Re*. Consider, for example, plasma spraying of molybdenum powder particles

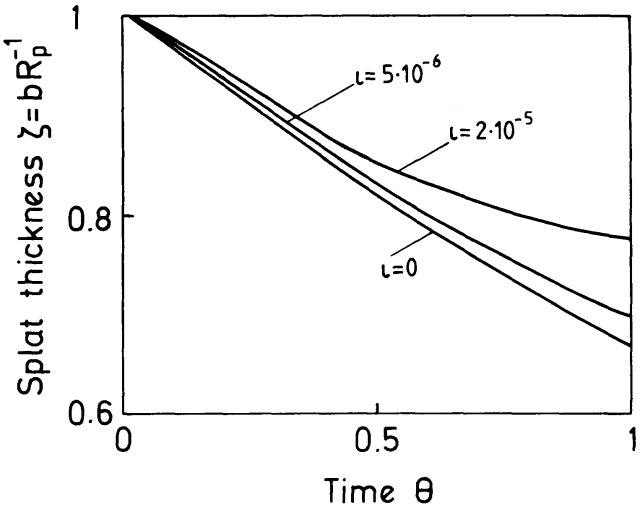

Fig. 5 Influence of substrate deformation on variation of splat thickness with time (Ref 23)

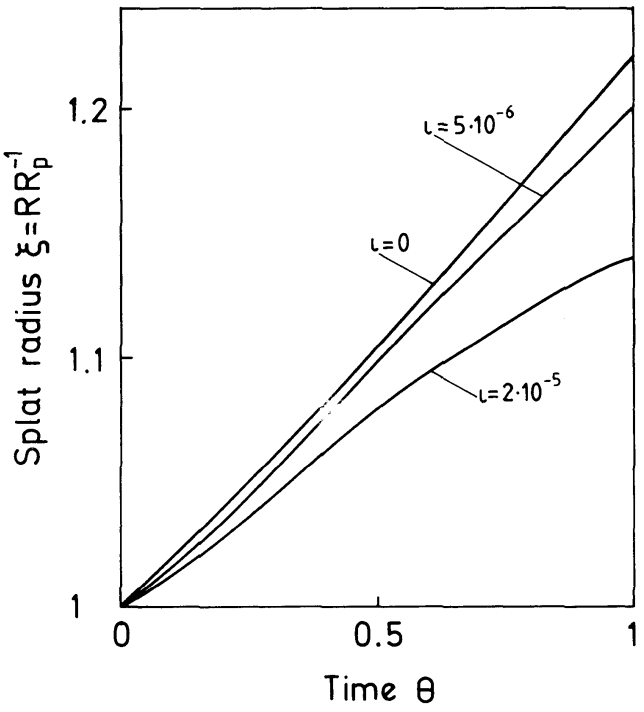

Fig. 6 Influence of substrate deformation on variation of splat radius with time (Ref 23)

when Re = 30,000 (R_p = 20 μm and U = 150 ms^{-1}) and ι = 0.1 m^{-1}. Then ψ_3 = 0.81. Hence, in this case the value of θ_f is approximately 20% less than the time $\theta_{0.9}$.

The time, t_{fr}, of finishing of the flattening process due to the substrate roughness is given by Eq 10. When Re = 30,000 and α = 0.1, the ratio $\psi_r = t_{fr}/t_f$ is equal to 0.58. Thus, the substrate roughness may hinder flattening more intensively than the positive curvature of the substrate. This tendency is not so pronounced when solidification of the lower part of the splat occurs during flattening because the solidification process can be shown to increase the value of θ_{fr}.

Experimental analyses of effects of the substrate nature on the droplet flattening were presented in Ref 24 and 25. The experiments undertaken in Ref 26 with different substrate materials (glass, steel, and copper) showed that the Young's modulus of the substrate influenced the flattening process of the impinging droplets. The splat diameter was reported to increase with an increase in the substrate Young's modulus; that is, with a transition from glass to steel and further to copper. In Ref 25 a similar tendency was observed with the glass substrate and the molybdenum substrate. This occurred due to a decrease in the elastic response of the substrate, which was accompanied by a corresponding decrease in the droplet energy dissipated into the substrate during the impact and an increase in the energy available for the flattening process (Ref 24).

An increase in the Young's modulus of the substrate leads to a decrease in the substrate curvature (Ref 26) and this, according to Eq 17 results in an increase of the splat diameter. In Ref 24 and 25 there are not enough data to provide a quantitative comparison between the theoretical and experimental results. But it is possible to conclude that the results obtained agree with the experimentally observed tendencies of the splat flattening on different substrates.

4. Splat-Substrate Mechanical Interaction

Generation of high pressure at the impact zone during droplet flattening is an important factor for the development of the substrate-coating microadhesion (Ref 9, 20, 25) as well as the coating porosity (Ref 9, 10-12). Experimental data show that molten liquid impacting onto glass substrates produce small (5 to 10 μm) pits (Ref 27). This clearly indicates that the pressure generated upon impact has an essential influence on the splat-substrate mechanical interaction in thermal spraying. The process of pressure generation was studied numerically in Ref 28 and 29 and analytically in Ref 6, 7, 22, and 30.

The numerical solution of the complete Navier-Stokes equations based on the modified SOLA-VOF method obtained in Ref 29 shows that right after the impact, pressure at the regions close to the substrate increases to a very high value (150 MPa). This pressure decreases in the direction of the free surface of the droplet. As the droplet spreads on the substrate, the pressure decreases very quickly, and in less than 1 μs the pressure all over the splat reduces close to the ambient pressure. Very high pressure lasts approximately 0.1 μs.

Analysis undertaken in Ref 28 by means of numerical solution of the full Navier-Stokes equations indicates that the material density, the particle impact velocity, and the particle diameter are the main factors governing the development of the pressure. The pressure increases with an increase of these parameters and after the impact increases up to 400 to 600 MPa. At the early stage of the droplet spreading, the viscous force is negligible in comparison with the inertial force, and the viscosity of the droplet material is shown to have no significant effect on the pressure generation.

For engineering practice it is necessary to have simple formulas to estimate the generation of high pressure. Although these formulas are approximate they reflect all the main features of the process and allow understanding of the formation of the substrate-coating microadhesion and coating porosity. Such analytical formulas agree well with the experimental data (Ref 22). The main analytical results are given in the following paragraphs.

In the center of the droplet the impact pressure, P_{im}, is determined by the compressibility effects and can be presented as (Ref 31):

$$P_{im} = 0.5\gamma_1 \rho c U \qquad \text{(Eq 18)}$$

where c is the sound velocity in the impinging droplet. The value of the coefficient, γ_1, in general can be found empirically. At very high impact velocities corresponding to thermal spraying the coefficient, γ_1, can be taken as unity (Ref 22, 31).

In the central part of the impinging droplet within the distance $r = r_m$ from its center of approximately 0.1 μm, the mean value of the pressure, P_a, with respect to the droplet height can be presented as:

$$P_a = P_0 - \mu F b^2 r^{-3}/3 + U R_p^{-1} \rho F b^2 r^{-1}/3 \qquad \text{(Eq 19)}$$

where $F = U \exp(-UR_p^{-1}t)$. From Eq 19 it follows that at $r = r_m$, P_a has the value P_m:

$$r_m = 2.45 R_p \, Re^{-1/2} \qquad \text{(Eq 20)}$$

$$P_m = P_0 + \Delta P \qquad \text{(Eq 21)}$$

where in Eq 20 $Re = 2R_p U \rho \mu^{-1}$. In Eq 21 $\Delta P = 0.09 \rho U F b^2 R_p^{-2} Re^{1/2}$. From Eq 19 and 21 it follows that an increase in the droplet velocity, U, and density, ρ, leads to a decrease in r_m and an increase in P_m. Therefore, an increase in the kinetic energy of the droplet causes an increase in the pressure impulse generated upon impact and makes it closer to the splat center. Thus, the pressure variation becomes sharper.

The flow viscosity during the droplet impact and flattening can be increased effectively due to factors such as cavitation developed during flattening (Ref 31), the roughness of the substrate surface (Ref 14), and the rheological properties of the droplet material in the thermal interval of solidification. Viscosity increases effectively when cavitation occurs due to additional radiative and thermal losses of energy caused by gas bubbles (Ref 32, 33). The flow viscosity also increases effectively when the droplet flattening occurs at a rough surface due to additional deceleration of the flow (Ref 14). Rheological behavior of the droplet material manifests in an increase of the flow viscosity due to the processes of relaxation and retardation of the flow motion (Ref 34, 35). An increase in μ gives rise to an

increase in the dissipation of the droplet energy and hence to a decrease in P_m and an increase in r_m.

Under the thermal spray conditions *Re* is very high ($Re = 10^4$ to 10^5) (Ref 4, 9). For example, when $Re = 30{,}000$, it can be obtained from Eq 20 that $r_m = 0.01R_p$. Thus r_m has the order of 10^{-7} m and does not exceed 1 μm. Thus, the value of r_m corresponds approximately to the lower limit of the interval of r where the formula in Eq 19 for P_a is valid. Hence the radial variation of the pressure according to Eq 19 can be considered starting from $r = r_m$.

For thermal spraying it is important to know the final values of the droplet pressure at $t = t_f$ when the flattening can be considered to be complete. When $Re >> 1$, the value of t_f is obtained (Ref 1, 16). The maximum increase in pressure is (Ref 22):

$$\Delta P = 0.11\rho U^2 Re^{1/3}[1 + 0.24\alpha^{1/2} Re^{1/2} - 1.36\beta\ Re^{1/2} \ln(0.3\,Re)] \quad \text{(Eq 22)}$$

This formula shows that the maximum pressure increases with an increase in the surface roughness and decreases with an increase in the solidification velocity in the lower part of the splat. The value of ΔP is also enhanced by the Reynolds number.

During droplet flattening on a smooth surface ($\alpha = 0$) with very small influence of the solidification process ($\beta = 0$) $P_m = P_0 + 0.11\rho U^2 Re^{1/3}$. It is worth comparing this maximum pressure with the impact pressure P_{im} (Ref 31). The ratio $Y = P_m/P_{im}$ can be written as $Y = 0.22Uc^{-1}Re^{1/3}$. Under the typical parameters corresponding, for example, to the plasma spraying of metallic powders when $U = 150$ ms^{-1}, $Re = 30{,}000$, and $c = 3000$ ms^{-1}, $Y = 0.34$. Thus, the pressure distribution upon impact can be presented as follows. In the very center of the droplet this pressure is maximum and equal to P_{im}. Within the distance of approximately 0.1 μm the pressure decreases almost to 1/2 the value of P_m and then decreases according to the formula in Eq 19. Assuming $r = \eta R(\eta < 1)$ the following approximate formula for the pressure P_a is obtained:

$$P_a = P_0 + 0.48\rho U^2 \eta^{-1}\chi^{-1/2} Re^{-5/12}[1 + 0.3\alpha^{1/2} Re^{1/2} - 1.7\beta\, Re^{1/2} \ln(0.3\,Re)] \quad \text{(Eq 23)}$$

When the surface is smooth ($\alpha = 0$) and splat solidification is negligible ($\beta = 0$), it is obtained from Eq 23 that $P_a = P_0 + 0.48\rho U^2 \eta^{-1}\chi^{-1/2} Re^{-5/12}$. The formula in Eq 23 is valid when $r = \eta R >> r_m = \eta_c R$ or $\eta >> \eta_c$. From Eq 23 $\eta_c = 2.45 Re^{-1/2} R_p R^{-1}$. When, for example, $Re = 30{,}000$ and the flattening degree $RR_p^{-1} = 5$, $\eta_c = 0.003$. Therefore, the formula in Eq 23 can be used to estimate the splat pressure everywhere with an exception of the central part of the splat where r is approximately 0.1 μm. In the latter region the formulas in Eq 18 and 21 must be used.

One of the main applications of the information of pressure distribution during droplet flattening is concerned with the possibility of predicting substrate-coating microadhesion. Usually the substrate surface is rough and even; even if it is considered smooth, some small roughness always exists. To have good adhesion it is necessary to put the surfaces of the substrate and the coating into close contact. This can be done at the very high pressure developed during the droplet flattening. To obtain such close contact this pressure must exceed the capillary pressure, P_σ, which arises at the substrate-coating interface due to the roughness (Fig. 7). Capillary pressure can be estimated as $P_\sigma = 4\sigma\varepsilon^{-1}$, where σ is the surface tension coefficient. An important parameter is the ratio, ζ, of the dynamic pressure, P_a, to the capillary pressure P_σ: $\zeta = P_a/P_m$.

From Eq 23 it follows that the substrate-coating microadhesion increases with an increase in the density and velocity of the impinging droplet and the roughness of the substrate surface. Microadhesion decreases with an increase in the droplet mass loss upon impact and the surface tension at the substrate-droplet interface. Substrate-coating microadhesion is maximum in the central part of the splat and diminishes in the direction of its periphery. These tendencies correspond to those found experimentally during thermal spraying (Ref 25).

Thus, good substrate-coating microadhesion can be expected when $\zeta \geq 1$ or when $r \leq r_e = \eta_e R$ where η_e is such value of η, which corresponds to $\zeta = 1$. This means that the pressure developed during the droplet impact exceeds the capillary pressure until $r \leq r_e$.

Figure 8 illustrates the behavior of ζ for plasma sprayed molybdenum particles when $Re = 20{,}000$, $U = 150$ ms^{-1}, $\rho = 9900$ kgm^{-3}, $\sigma = 2.5$ Nm^{-1}, $\chi = 1$, and $\varepsilon = 0.2$ μm. The radius, r_e, of the zone of good adhesion increases with an increase in the substrate roughness and decreases with an increase in the solidification velocity in the lower part of the splat.

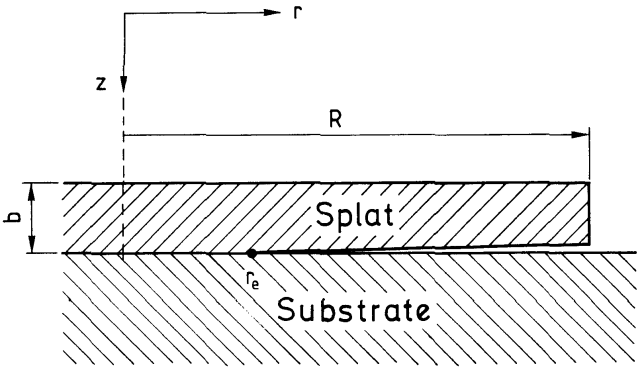

Fig. 7 Final stage of droplet impingement onto a substrate surface

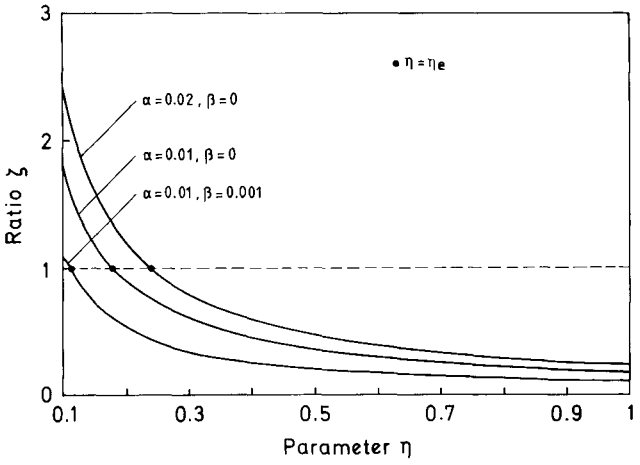

Fig. 8 Variation of ratio ζ along the droplet-substrate interface (Ref 22)

The experimental data concerning plasma spraying of molybdenum powder particles onto glass and molybdenum substrates show that only the central part of the molybdenum splat adheres to the substrate surface. This part represents less than 10% of the initial particle volume (Ref 25).

According to the equation of droplet mass conservation during flattening (Ref 1), when $V_s = 0$, in this case $r_e = 0.3\,R$ and $\eta_e = 0.3$. Intersections of the line $\zeta = 1$ with the curves in Fig. 8 give $\eta = \eta_e$. It is seen that $\eta_e < 0.3$, and this agrees well with the experimental results presented in Ref 23.

The influence of the substrate deformation on the splat-substrate mechanical interaction is analyzed in Ref 23. The concave form of the substrate is shown to cause an increase in r_m and a decrease in P_m. Thus, an increase in the positive substrate curvature leads to a decrease in pressure generated upon the droplet impact and to a more uniform distribution of this pressure. Such a situation occurs because in this case some part of the kinetic energy of the impinging droplet is used for deformation of the substrate and the rest of the kinetic energy, which contributes to the development of pressure decreases.

From the results obtained in Ref 23 it follows that an increase in the positive substrate curvature gives rise to a decrease in the value of r_c and, hence, to a decrease in the central area of the splat where good adhesion between the coating and the substrate and poor coating porosity can be observed.

The previously mentioned results can be also applied to the situation when the impinging droplets are not deposited onto the substrate surface but onto already deposited coating layers.

5. Dynamics of Splashing

Splashing plays a key role in the splat formation (Ref 19, 24, 36). Splat-substrate interaction and solidification of the lower part of the splat is reported to be a critical issue for splashing (Ref 19, 20, 37-40).

The experimental results show that on a smooth surface splashing occurs at low substrate temperatures, T_s, and does not occur at higher temperatures. A transition substrate temperature, T_{tr}, is shown to exist for different substrate materials (Ref 19, 41, 42). This temperature defines the thermal interval of splashing in such a way that splashing occurs when an initial temperature of the substrate, T_{so}, is lower than T_{tr}. Splashing is absent when $T_{so} = > T_{tr}$ (Fig. 9). Splashing occurs more easily on a rough surface of the substrate (Ref 2, 36). It does not occur when the splat

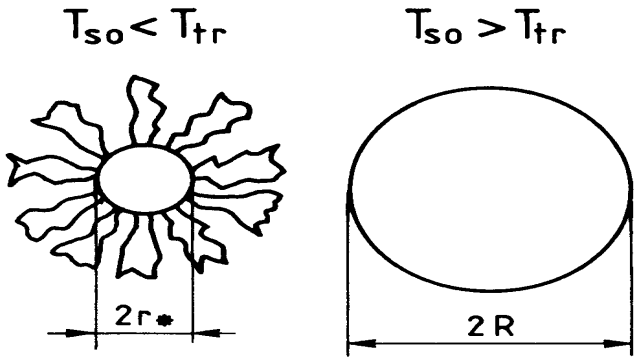

Fig. 9 Scheme of formation of splats on a smooth substrate surface with splashing ($T_{so} < T_{tr}$) and without splashing ($T_{so} > T_{tr}$)

radius, R, is in a certain interval of values depending of the spacing of roughness (Ref 36). This article follows Ref 20 and 41 to give the main results of an analysis of the mechanisms of the development of splashing during thermal spraying.

5.1 Splashing on a Smooth Surface

The splashing observed on a smooth substrate surface can be explained as follows: High pressure developed upon the droplet impact contributes to establishing close contact between the substrate and the central part of the splat where $r = \leq r_*$. This pressure causes an increase in the melting point, T_k, of the liquid phase of the droplet and development of a supercooling ΔT_p in addition to a thermal supercooling ΔT_h created by cooling due to the heat removal from the splat (Ref 37, 38).

The contact thermal resistance, R_c, at the substrate-splat interface slows down heat transfer from the splat to the substrate and, hence, a cooling velocity, V_c, of the liquid splat. As a result under a low initial temperature, T_{so}, of the substrate, the supercooling ΔT_h could be insufficient for crystallization of the splat to occur, and the main contribution to the total supercooling would be ΔT_p. In this case the splat crystallization will occur in the region of the best contact between the splat and the substrate where $r = \leq r_*$. Due to this, the form of the central part of the splat will be kept regular (disk-shaped). Splashing will occur when $r = \geq r_*$ and splash-shaped (finger-shaped) splats will form (Ref 36).

An increase in the initial temperature of the substrate, T_{so}, leads to a decrease in the contact thermal resistance, R_c (e.g., due to decomposition of impurities at the interface), and to an increase in the heat removal from the splat (Ref 25). Then the value of ΔT_h increases. When T_{so} attains the transition (critical) value, T_{tr}, the supercooling achieves its critical value ΔT_*. This allows solidification of the whole splat to occur. This leads to an increase in the splat radius, R, and formation of regular disk-shaped splats (Ref 19, 42). Note that ΔT_p is important mostly in the central part of the splat where high pressure is developed and becomes less important at the periphery of the splat when the pressure decreases (Ref 22). Supercooling ΔT_p can be estimated as (Ref 15):

$$\Delta T_p = T_k P(\rho q_p)^{-1} \qquad \text{(Eq 24)}$$

where T_k is the melting point of the droplet material.

Pressure developed in the central part of the splat can be presented in a form of Eq 22 (Ref 22). For example, in the case of plasma spraying of zirconia with the same parameters as previously mentioned, it is obtained from Eq 22 that $P = 3.18 \cdot 10^8$ Nm^{-2} and $\Delta T_p = 229$ °C for $R_p = 15$ μm, $\sigma = 0.5$ Nm^{-1}, and $\varepsilon = 0.05$ μm. The value of ΔT_p is even higher as the pressure increases T_k. Supercooling ΔT_h is developed due to removal of the heat from the splat to the substrate with the heat flux, q, which can be estimated as follows: $q = \alpha_c (T_{sp} - T_{sb})$, where T_{sp} and T_{sb} are the temperatures of the splat and the substrate respectively at the interface, and α_c is the contact heat transfer coefficient at the substrate-splat interface ($\alpha_c = R_c^{-1}$). Taking into account that $T_{sp} = T_k + \Delta T_{oh}$ and $\Delta T_h = T_k - T$, where ΔT_{oh} is an initial overheating of the splat and T is a current temperature of the splat, the equation for the supercooling ΔT_h is:

$$\Delta T_h = T_{sb} + q\alpha_c^{-1} - \Delta T_{oh} - T \quad \text{(Eq 25)}$$

Total supercooling ΔT is equal to the sum of ΔT_p and ΔT_h:

$$\Delta T = \Delta T_h + \Delta T_p \quad \text{(Eq 26)}$$

Beginning the process of crystallization of the splat it is necessary to achieve embryos of crystallization with a critical size, r_k, which are formed due to supercooling. During the growth of a spherical embryo the following heat, Q_1, is released: $Q_1 = 4\pi r_k^3 q_p \rho/3$.

It is considered that the density of the liquid phase of the splat is equal to that of the solid phase. Due to Q_1, the heating of the spherical layer $r_k \le r \le r_1$ around the embryo takes place from a current temperature, T, to a temperature, T_1, which should not exceed T_k. The following heat, Q_2, is spent for this heating: $Q_2 = 4\pi(r_1^3 - r_k^3)\rho c_1 \delta T/3$ where $\delta T = T_1 - T$ and c_1 is the specific heat of the splat material. From the balance equation $Q_1 = Q_2$, $r_k^3 q_p = c_1 \delta T(r_1^3 - r_k^3)$ is obtained. The value of δT can be presented as: $\delta T = \Delta T - \Delta_1 T$, where $\Delta_1 T = T_k - T_1$ and $\Delta_1 T$ characterizes approaching the temperature T_1 to T_k, that is, decreasing of the supercooling due to release of the latent heat of fusion. Then, $\Delta_1 T = \Delta T - q_p r_k^3 [c_1(r_1^3 - r_k^3)]^{-1}$. To have $\Delta_1 T = >0$ it is necessary for the supercooling ΔT to exceed some critical value ΔT_c. This value is obtained when $\Delta_1 T = 0$:

$$\Delta T_c = q_p[c_1(r_1^3 r_k^{-3} - 1)]^{-1} \quad \text{(Eq 27)}$$

For example, in the case of plasma spraying of zirconia, $q_p = 0.71 \cdot 10^6$ Jkg^{-1} and $c_1 = 604$ J (kgK)$^{-1}$ (Ref 39). Taking $r_1 = 1.9 r_k$, from Eq 27, $\Delta T_c = 201$ °C. Thus, when the supercooling ΔT in the splat liquid phase attains the value of ΔT_c, the splat solidification starts in the lower part of the splat, extends in the direction of the upper surface of the splat, and influences splashing.

The time for establishing supercooling is about the characteristic time, t_d, of the heat diffusion in the lower part of the splat with a thickness δ, that is $t_d = \delta^2 a^{-1}$, where a is the thermal diffusivity of the splat material. The value of t_d must be compared with the characteristic impact time $t_{im} = R_p U^{-1}$. The ratio Ω_1 of t_d to t_{im} is $\Omega_1 = \delta^2 U (aR_p)^{-1}$.

In the case of plasma spraying of zirconia coatings with a thickness, b, when $a = 6.7 \times 10^{-6}$ m^{2}s^{-1}, $\alpha = 0$, $\beta = 0$, and $\delta = 0.2b$, from Ref 14 and 17, $b = 0.8$ μm and $\Omega_1 = 0.5$. Thus, critical supercooling is established during the droplet impact, and solidification influences splashing and droplet flattening. Under high supercooling crystal growth occurs according to the relation between the critical velocity of solidification, V_{kc}, and the critical supercooling ΔT_c. From Ref 40 $V_{kc} = K(\Delta T_c)^2$, where K is the empirical coefficient. Taking into account that a cooling velocity in the splat can be presented as $V_c = V_k G$, where G is the thermal gradient, the following equation for the critical cooling velocity, V_c, is:

$$V_{cc} = G(K\Delta T_c)^2 \quad \text{(Eq 28)}$$

Thus, the critical supercooling in the splat is achieved when $V_c = V_{c*}$, and solidification of the splat takes place if $V_c = \ge V_{cc}$. Using Eq 28 it is also possible to estimate the value of ΔT_c when the critical cooling velocity is known. Supercooling can also be presented as:

$$\Delta T = V_c[(GK)^{-1}]^{1/2} \quad \text{(Eq 29)}$$

5.2 Splashing on a Rough Surface

Splashing on a rough surface depends on surface morphology, particularly on the average peak spacing, s. A valley of roughness on the substrate surface must be sufficiently wide to allow the splat to be flattened to its final diameter, $D = 2R$, or it will spill over the roughness peak into the next valley to form splashes (Ref 36). Therefore, the final diameter of the splat must be less than the spacing, s, between the peaks. If the value of D is much smaller than s, the impinging small droplets will strike the side of the valley and then run downhill to form splashes. Experiments show that to minimize splashing the splat diameter must be in the interval between s and 0.25 s (Ref 36): $0.25\ s < D < s$. Splashing occurs when D is outside this range. When it is inside, the kinetics of splashing are similar to that for the smooth surface.

5.3 Comparison with the Experimental Data

Consider plasma spraying of zirconia powder particles. From Ref 42 it follows that in this case the critical cooling velocity, V_{cc}, is equal to 5.48×10^8 Ks^{-1}. Taking $\Delta T_c = 201$ °C (as was found previously) and estimating G, which is equal to 10^7 Km^{-1} (Ref 42), it is obtained from Eq 28 that $K = 1.36 \times 10^{-3}$ m(Ks)$^{-1}$. Putting $V_c = V_{c1} = 1.4 \times 10^8$ Ks^{-1}, it is obtained from Eq 29 that $\Delta T = 101$ °C $< \Delta T_c$. When $V_c = V_{c2} = 6 \times 10^8$ Ks^{-1}, it is obtained from Eq 29 that $\Delta T = 210$ °C $> \Delta T_*$. The cooling velocity, V_{c1}, corresponds to $T_{so} = 348$ K, and the value of V_{c2} corresponds to $T_{so} = 573$ K (Ref 42). Therefore, the transition substrate temperature must correspond to $T_{so} = T_{tr}$, which is

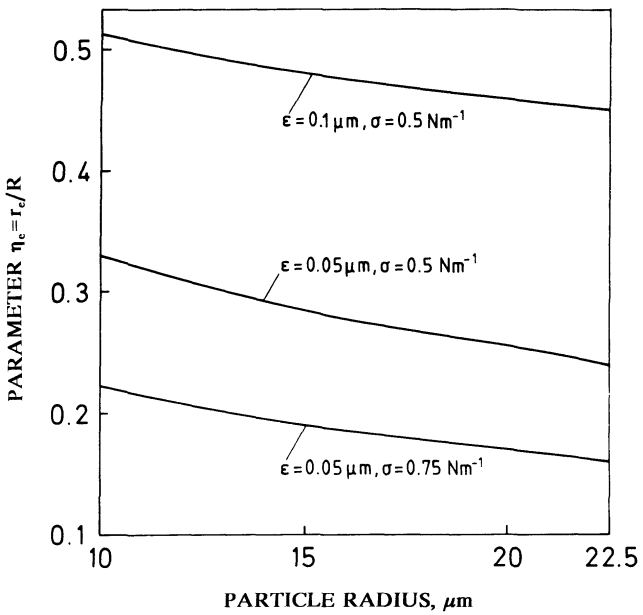

Fig. 10 Variation of parameter η_e with respect to particle radius (Ref 41)

between 348 and 573 K. It follows from Ref 42 that the value of T_{tr} = 523 K.

The substrates in Ref 42 exhibit a low roughness. With the "cold" substrate ($T_{so} = < T_{tr}$), as shown in Fig. 10, the central disk-shaped part of the splat can be considered to have a radius in the interval 0.16 to 0.51 *R*. With the "hot" substrate ($T_{so} = > T_{tr}$), no splashing occurs, and the value of *R* can be estimated from Part I (Ref 1) of this review. With ε = 0.05 μm and the parameters corresponding to plasma spraying of zirconia, from Part 1 *R* = 71 μm. This value of *R* is in the range of the experimentally observed values of *R*, which vary from 69 to 137 μm for the initial powder size distribution from 22 to 45 μm (Ref 42). Thus, the theoretical results agree with the experimental observations.

6. Spraying at Off-Normal Angles

Thermal spraying at off-normal angles is used in some special applications (e.g., development of the coating in the inner part of a pipe), and it can influence markedly the coating structure and properties (Ref 43-46). The coating quality depends significantly on the flattening of thermally sprayed droplets and the droplet-substrate mechanical interaction when the adhesive bonds are developed.

Plasma and flame spraying of alumina and molybdenum powders at angles ranging from 90 to 45° (with some measurements at 30°) was investigated in Ref 43, and measurable variations in deposition efficiency, surface roughness, and porosity over the angular range studied were reported to occur. In Ref 44 the effect of different deposition angles in the range from 90 to 30° on the properties of tungsten carbide-cobalt coatings sprayed by detonation gun and plasma techniques was studied. Tucker and Price (Ref 44) stated that some changes in microstructure were detected at low angles of deposition, and there appeared to be little change in coating hardness, strain to failure, alumina erosion, or low stress abrasion resistance as a function of angle of spraying between 90 and 45°.

An investigation of the effects of droplet impact angle in atmospheric plasma spray deposition of aluminum, aluminum oxide, copper, 95Ni-5Al alloy, and molybdenum powders onto type 304 stainless steel plates has been undertaken (Ref 45). Also aluminum wire was deposited by single-wire plasma, twin-wire arc, and combustion flame spray processes. It was shown that the deposition efficiency and coating porosity started to change markedly at φ = 45°. Substantial changes in deposition efficiency and coating porosity that could affect coating properties and process performance were observed at φ = 30° for many of the cases studied. On the basis of these observations Smith, Neiser, and Dykhuizen (Ref 45) conclude that the angle φ = 45° can be recommended as a general limit for off-normal thermal spraying for achieving quality coatings.

In Ref 46 the influence of the substrate orientation on the coating formation was studied for the vacuum plasma spray forming of astroloy. It was shown that the spray angle had an essential effect on the splat morphology and deposit characteristics including the porosity level, the deposition efficiency, the deposit thickness, and the microhardness.

Engineering practice requires simple formulas that permit estimation of these processes. Much has been done in relation to the flattening of droplets during thermal spraying at normal angles (Ref 2, 17), However, quantitative information about the influence of thermal spraying at off-normal angles on droplet flattening and droplet-substrate mechanical interaction is necessary. This information includes formulas describing the time evolution of the splat thickness, *b*, splat radius, *R*, rate characteristics, *db*/*dt*, *dR*/*dt*, and pressure, *P*, developed and the dependence of the final values of these parameters on the Reynolds number, *Re*, taking into account a droplet impact angle, φ. These analytical results, which are in agreement with the experimental data, were obtained in Ref 30 and 47.

Consider a droplet of radius, R_p, impinging under an angle φ (between a substrate and the centerline axis of the spraying gun) onto the substrate surface and forming a cylindrical splat (disk) of radius, *R*, and thickness, *b*, which vary with time, *t*, during flattening. The splat circularity (a shape factor of elongation, unity being a perfect circle) decreases with a decrease in the spray angle, φ, and an assumption on the splat circularity can be considered reasonable up to φ, approximately 45° (Ref 46).

As was established in Ref 30 and 47 the mean pressure in the splat P_a is given by the formula:

$$P_a = P_0 - \mu F b^2(3 - \cos\varphi)/(9r^3) + a\rho F b^2(1 - \cos\varphi)/(3r) \quad \text{(Eq 30)}$$

From Eq 30 it follows that the pressure has the value, P_m, at the distance $r = r_m$ of approximately 0.1 μm:

$$r_m = R_p(1 - \cos\varphi)^{-1}[2\,Re_*^{-1}(3 - \cos\varphi)]^{0.5} \quad \text{(Eq 31)}$$

$$P_m = P_0 + \Delta P \quad \text{(Eq 32)}$$

where $\Delta P = 0.157\rho U_n F b^2 R_p^{-2}\,\mathrm{Re}_*^{-0.5}(1 - \cos\varphi)^2(3 - \cos\varphi)^{-0.5}$

$Re_* = Re\,\psi_o(\varphi)$

$Re = 2R_p|U|\rho\mu^{-1}$

$\psi_o = \sin\varphi\,(1 - \cos\varphi)^{-1}$

and where Re_* is an effective Reynolds number depending on φ. Because the splat circularity can be considered to occur when 90° ≤ φ ≤ 45°, the value of ψ_o varies from 1 to ~2.4.

When φ = 90°, from Eq 31 and 32 the formulas for r_m and P_m are obtained, corresponding to thermal spraying at normal angles (Ref 22). From Eq 31 and 32 it follows that the value of r_m increases and the value of P_m decreases with a decrease in φ. Therefore, as the thermal spraying angle decreases, the maximum pressure developed during the droplet impact decreases, and the location of the maximum is displaced outward toward the splat periphery. Thus, the radial pressure distribution becomes more uniform than for spraying normal to the substrate surface (90°).

Using Eq 32 the following equation is obtained for the final value of the maximum increase in pressure ΔP_f:

$$\Delta P_f = 0.116\rho_p|U|^2 Re^{0.75}\eta_1(\varphi) \quad \text{(Eq 33)}$$

where $\eta_1(\varphi) = \sin^{2.75}\varphi(1 - \cos\varphi)^{1.25}(3 - \cos\varphi)^{-0.5}$.

The value of ΔP_f is maximum at φ = 90° and decreases with a decrease in the spraying angle. The final splat thickness, radius, and rate characteristics have the form:

$$\zeta_f = 1.826\, Re_*^{-1/2} \quad \text{(Eq 34)}$$

$$\xi_f = 0.8546 \chi_*^{1/2} Re_*^{1/4} \qquad \chi_* = \chi \sin\varphi \quad \text{(Eq 35)}$$

When $\varphi = 90°$ the formulas describing the flattening characteristics during thermal spraying at normal angles are obtained when $\alpha = 0$ and $\beta = 0$. Figures 11 and 12 show variations of spraying parameters with respect to *Re* and φ. A decrease in the spraying angle, φ, causes a decrease in the normal component, U_n, of the droplet velocity, U ($U_n = |U|\sin\varphi$). According to the theoretical and experimental data available this contributes to a decrease in the final splat thickness ζ_f (Ref 45) and hence to an increase in the final splat radius, ξ_f. On the other hand, a decrease in φ leads to a decrease in the radial component, V_r, of the flow velocity, V, and the velocity of spreading of a droplet. This contributes to an increase in ζ_f and a decrease in ξ_f. Finally a geometrical factor $\psi_o(\varphi)$ increases with a decrease in the spraying angle φ.

Thus, during thermal spraying at off-normal angles the effective Reynolds number, Re_*, increases with a decrease in φ. Therefore, the final splat thickness, ζ_f, decreases when φ decreases (Ref 47). The final splat radius ξ_f depends also on the effective splashing factor χ_*. Because this factor decreases with an increase in φ and the geometrical factor, $\psi_o(\varphi)$, increases when φ increases, the behavior of ξ_f in general is nonuniform with respect to φ. When the spraying angle decreases these flattening characteristics increase, and at $\varphi = \varphi_m$ they reach the maximum values. The further increase in φ leads to a decrease in ξ_f (Ref 47).

From Eq 35 it follows that $\varphi_m = 60°$. The value of ξ_f increases when φ decreases from 90 to 60°, has the maximum at $\varphi = 60°$, and then decreases as φ increases. The value of ξ_f at $\varphi = 45°$ is less than at $\varphi = 60°$ and is very close to that at $\varphi = 75°$. For this reason it cannot be shown properly in Fig. 12.

The pressure developed during the impact of the droplet influences the droplet-substrate microadhesion. To obtain good adhesion, it is necessary to force the surfaces of the substrate and the droplet together. The very high pressure developed during the droplet impact and flattening makes this possible. It can be shown that the substrate-droplet microadhesion decreases with a decrease in the spraying angle φ (Ref 30). Therefore, microadhesion is maximum during spraying at normal angles when $\varphi = 90°$.

Gas porosity formed in thermal spray coatings can be decreased by applying high pressure, which is developed upon the droplet impact (Ref 10-12). This pressure must exceed mostly the capillary pressure at the gas-liquid droplet interface, which is significantly greater than the atmospheric pressure. The radius of pores, R_{pr}, can be approximated using the following equation (Ref 11):

$$R_{pr} = R_0[2\sigma R_0^{-1}(P_a + 2\sigma R_0^{-1})^{-1}]^{\Gamma} \quad \text{(Eq 36)}$$

where $\Gamma = (3\upsilon)^{-1}$, R_0 is the radius of a gas bubble in a liquid splat, which after solidification is transformed in a pore, and υ is the specific heat ratio. From Eq 36 it follows that the pore size is minimum at $\varphi = 90°$ and increases with a decrease in the spraying angle. As $P_0 << \Delta P$, the final value of the pressure, P_a, can be taken equal to the final value of ΔP. This value of ΔP exceeds

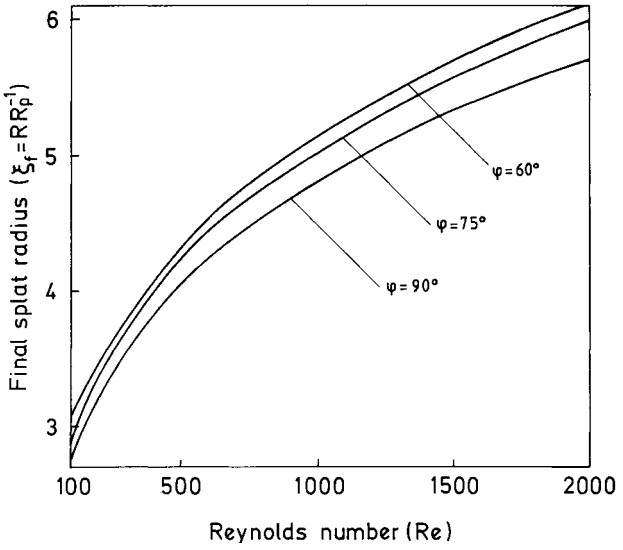

Fig. 12 Variation of final splat radius with the Reynolds number at different spraying angles (Ref 47)

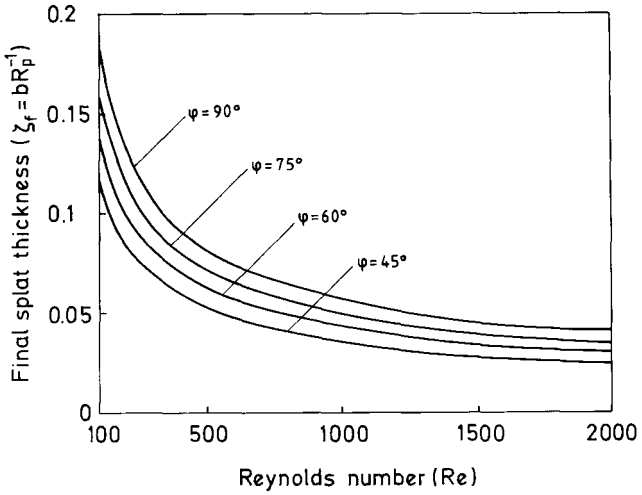

Fig. 11 Variation of final splat thickness with the Reynolds number at different spraying angles (Ref 47)

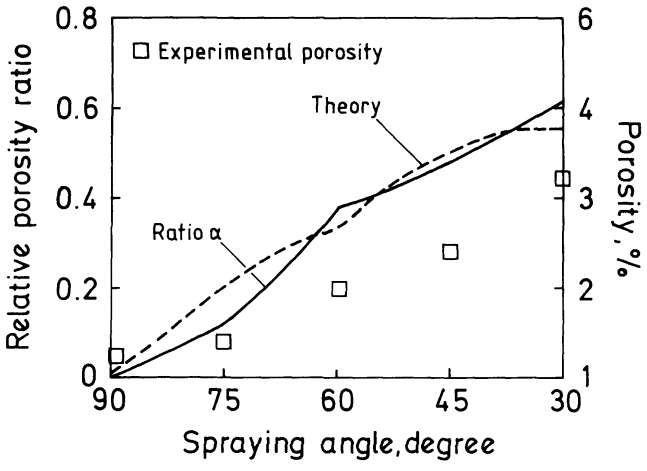

Fig. 13 Variation of relative porosity with respect to spraying angle (Ref 30)

the capillary pressure term, and the latter can be neglected in the denominator of Eq 36. Thus, from Eq 36:

$$RR_0^{-1} = (2\sigma P_a^{-1} R_0^{-1})^{\Gamma} \quad \text{(Eq 37)}$$

Under an assumption that the number of pores remains the same at different pressure conditions, the parameter $R\,R_0^{-1}$ depending on φ can be considered as a relative porosity. From Eq 37 it follows that the ratio, *E*, of the difference between the values of this parameter at any spraying angle, φ, and at normal angle 90° to that determining relative porosity at any spraying angle, φ, in terms of the pressure is:

$$E = \{[P_a(90°) - P_a(\varphi)]/P_a(90°)\}^{\Gamma} \quad \text{(Eq 38)}$$

The ratio, *E*, in Eq 38 increases with a decrease in φ. Figure 13 presents the values of *E* calculated for different angles. In the same figure a fit to the experimental values of the relative porosity of the aluminum coatings plasma sprayed onto a stainless steel and the experimental values of the relative porosity are given. The experimental data were taken from Ref 45. The theoretical results are seen to be in a reasonable agreement with the experimental observations at off-normal angles between 30 and 90°.

Montavon et al. (Ref 46) showed that the deposit thickness decreases with an increase in φ. When the spraying angle changes from 90 to 45° the deposit thickness decreases by a factor of approximately three. From Fig. 11 it follows that the final splat thickness, ζ_f, decreases by a factor of approximately 1.5 when φ changes from 90 to 45 °. It could be assumed that the deposit thickness, which includes many splats, is more sensitive to the variations of φ and is subjected to a larger decrease.

The conclusion of Ref 45 that the 45° angle can be recommended as a reasonable limit for off-normal thermal spraying for the development of the quality coatings is also supported by the results. It was shown that the final splat radius attained the maximum value at φ = 60°, then decreased when φ enhanced. Its value at φ = 45° differed insignificantly from that at φ = 60°. Thus, the angle φ = 45° can be recommended as a reasonable limit for off-normal thermal spraying for achieving the quality coatings.

7. Conclusions

A decrease in the contact wetting angle between the splat and the substrate leads to a decrease in the splat thickness and an increase in the splat radius that contributes to reinforcement of the splat-substrate adhesive bonding. The splat porosity increases with an increase in the contact wetting angle. Influence of wetting on the flattening process decreases with an increase in the velocity of the droplet impingement onto the substrate surface and a decrease in the substrate initial temperature.

The analytical results, taking into account the surface effects, give an underestimated value of the final splat thickness and overestimated values of the final splat radius and the characteristic time of finishing of flattening. It follows that it is necessary to use the analytical results based upon the prime influence of the viscous effects on the flattening parameters.

The approximate formulas describing the time evolution of the splat thickness and radius during the flattening process and the pressure developed on the droplet impact are established taking into account the substrate deformation. The positive substrate curvature leads to an increase in the splat thickness and to a decrease in the splat radius and the pressure developed. The time of finishing of the flattening process is obtained, which is less than the same time in the case when the substrate deformation is absent. The surface roughness is shown to hinder flattening more intensively than the positive curvature of the substrate.

Droplet-substrate microadhesion and coating porosity are shown to depend significantly on the ratio between the pressure developed upon impact and the capillary pressure. Microadhesion is found to be maximum in the central part of the splat and to decrease in the direction of its periphery, while coating porosity is shown to be minimum in the central part of the splat and to increase toward its periphery. Droplet-substrate microadhesion increases with an increase in the density and velocity of the impinging droplet and the roughness of the substrate surface. Microadhesion decreases with an increase in the droplet mass loss upon impact and the surface tension at the droplet-substrate interface. Coating porosity demonstrates an opposite behavior with respect to the previously mentioned parameters.

Supercooling established in the flattening droplet is shown to consist of thermal supercooling and supercooling formed due to high pressure developed upon the droplet impact. Solidification starts when the supercooling exceeds the critical value corresponding to the critical value of the cooling velocity, which in turn corresponds to the critical (transition) initial temperature of the substrate. With the "cold" smooth substrate when T_{so} is $<T_{tr}$, the marked contribution to supercooling is due to its high pressure part. In this case a disk-shaped splat is formed in the central part, then splashing occurs, and the splash-shaped splats are formed at the periphery. With the "hot" smooth substrate (T_{so} is $>T_{tr}$) the thermal supercooling is high enough to allow solidification in the lower part of the whole splat. As a result, no splashing occurs and a regular disk-shaped splat is formed. On a rough surface of the substrate splashing does not occur when the final splat diameter is in the certain range of values with respect to the average peak spacing of the surface roughness.

Analytical formulas describing variations of the final values of the splat thickness and splat radius with the Reynolds number and the spraying angle are established. In thermal spraying at off-normal angles the final splat thickness decreases with a decrease in the spraying angle. The final splat radius varies nonuniformly with a decrease in the spraying angle and attains the maximum value when this angle is 60 °. The 45° angle can be recommended as a reasonable limit for off-normal thermal spraying for achieving the quality coatings. An analytical formula for the droplet pressure during impact on a substrate surface predicts a decrease in pressure and a more uniform distribution with a decrease in the spraying angle. Substrate-coating microadhesion is predicted to be a maximum during spraying at normal angles and to decrease when the off-normal angle decreases. Coating porosity is a minimum during thermal spraying at normal angles and increases with a decrease in the spraying angle.

Acknowledgments

The authors are grateful to the Generalitat de Catalunya (project SGR 97-15) and CICYT (project MAT 96-0426) for financial support.

References

1. V.V. Sobolev and J.M. Guilemany, Flattening of Droplets and Formation of Splats in Thermal Spraying: A Review of Recent Work—Part 1, *J. Therm. Spray Technol.*, Vol 8 (No 1), 1999, p 87-101
2. R.C. Dykhuizen, Review of Impact and Solidification of Molten Thermal Spray Droplets, *J. Therm. Spray Technol.*, Vol 3 (No. 4), 1994, p 351-361
3. M. Pasandideh-Fard and J. Mostaghimi, Deformation and Solidification of Molten Particles on a Substrate in Thermal Plasma Spraying, *Thermal Spray Industrial Applications*, C.C. Berndt and S. Sampath, Ed., ASM International, 1994, p 405-414
4. J. Madejski, Solidification of Droplets on a Cold Substrate, *Int. J. Heat Mass Transfer*, Vol 19, 1976, p 1009-1013
5. C. Moreau, P. Cielo, and M. Lamontagne, Flattening and Solidification of Thermally Sprayed Particles, *J. Therm. Spray Technol.*, Vol 1 (No. 4), 1992, p 317-323
6. V.V. Sobolev and J.M. Guilemany, Influence of Wetting and Surface Effects on Splat Formation during Thermal Spraying, *Mater. Lett.*, Vol 37, 1998, p 132-137
7. V.V. Sobolev and J.M. Guilemany, Effect of Oxidation on Droplet Flattening and Splat-Substrate Interaction in Thermal Spraying, *J. Therm. Spray Technol.*, 1999, (in press)
8. N. Eustathopoulos and B. Drevet, Mechanisms of Wetting in Reactive Metal/Oxide Systems, *Proc. Mater. Res. Symp., Mater. Res. Soc.*, Vol 314, 1993, p 15-26
9. L. Pawlowski, Science and Engineering of Thermal Spray Coatings, John Wiley & Sons, New York, 1994, p 324-360
10. H. Fukanuma, A Porosity Formation and Flattening Model of an Impinging Molten Particle in Thermal Spray Coatings, *J. Therm. Spray Technol.*, Vol 3 (No. 1), 1994, p 33-44
11. V.V. Sobolev and J.M. Guilemany, Investigation of Coating Porosity Formation during High Velocity Oxy-Fuel (HVOF) Spraying, *Mater. Lett.*, Vol 18, 1994, p 304-308
12. V.V. Sobolev and J.M. Guilemany, The Formation of the Coating Shrinkage Porosity in the Process of Thermal Spraying, *J. Mater. Process. Technol.*, Vol 58, 1996, p 227-232
13. G. Trapaga and J. Szekely, Mathematical Modeling of the Isothermal Impingement of Liquid Droplets in Spraying Processes, *Met. Trans.*, Vol 22B, 1991, p 901-914
14. V.V. Sobolev, J.M. Guilemany, and A.J. Martín, Influence of Surface Roughness on the Flattening of Powder Particles during Thermal Spraying, *J. Therm. Spray Technol.*, Vol 5 (No. 2), 1996, p 207-214
15. V.V. Sobolev, Influence of Cavitation on Metal Crystallisation under Ultrasonic Action on a Melt, *Comm. Acad. Sci. USSR Ser. Metals*, (No. 5), 1989, p 52-59
16. V.V. Sobolev and J.M. Guilemany, Flattening of Thermally Sprayed Particles, *Mater. Lett.*, Vol 22, 1995, p 209-213
17. V.V. Sobolev and J.M. Guilemany, Dynamic Processes during High Velocity Oxyfuel Spraying, *Int. Mater. Rev.*, Vol 41 (No. 1), 1996, p 13-32
18. V.V. Sobolev and J.M. Guilemany, Influence of Solidification on the Flattening of Droplets during Thermal Spraying, *Mater. Lett.*, Vol 28, 1996, p 71-75
19. M. Fukumoto, S. Katoh, and I. Okane, Splat Behaviour of Plasma Sprayed Particles on Flat Substrate Surface, *Thermal Spray—Current Status and Future Trends*, A. Ohmori, Ed., High Temperature Society of Japan, 1996, p 353-358
20. V.V. Sobolev, J.M. Guilemany, J. Nutting, and J.R. Miquel, Development of Substrate-Coating Adhesion in Thermal Spraying, *Int. Mater. Rev.*, Vol 42 (No. 3), 1997, p 117-136
21. H. Fukanuma, Mathematical Modeling of Flattening Process on Rough Surfaces in Thermal Spray, *Thermal Spray: Practical Solutions for Engineering Problems*, C.C. Berndt, Ed., ASM International, 1996, p 647-656
22. V.V. Sobolev and J.M. Guilemany, Droplet-Substrate Impact Interaction in Thermal Spraying, *Mater. Lett.*, Vol 28, 1996, p 331-335
23. V.V. Sobolev and J.M. Guilemany, Effect of Substrate Deformation on Droplet Flattening in Thermal Spraying, *Mater. Lett.*, Vol 35, 1998, p 324-328
24. G. Montavon, S. Sampath, C.C. Berndt, H. Herman, and C. Coddet, Effects of Substrate Nature on the Splat Morphology of Vacuum Plasma Sprayed Deposits, *Thermal Spray—Current Status and Future Trends*, A. Ohmori, Ed., High Temperature Society of Japan, 1996, p 365-369
25. C. Moreau, P. Gougeon, and M. Lamontagne, Influence of Substrate Preparation on the Flattening and Cooling of Plasma-Sprayed Particles, *J. Therm. Spray Technol*, Vol 4 (No. 1), 1995, p 25-33
26. T.W. Clyne and S.C. Gill, Residual Stresses in Thermal Spray Coatings and Their Effect on Interfacial Adhesion: A Review of Recent Work, *J. Therm. Spray Technol.*, Vol 5 (No. 4), 1996, p 401-417
27. E. Garrity, D. Wei, and D. Apelian, Modeling of Kinetics during Droplet Consolidation Processing, *Modeling of Casting and Welding Processes IV*, A.F. Giamei, Ed., The Minerals, Metals, and Materials Society, New York, 1988, p 593-602
28. G. Montavon, Z.G. Feng, C. Coddet, Z.Q. Feng, and M. Domaszewski, Influence of the Spray Parameters on the Transient Pressure within a Molten Particle Impacting onto a Flat Substrate, *Thermal Spray: A United Forum for Scientific and Technological Advances*, C.C. Berndt, Ed., ASM International, 1997, p 627-633
29. M. Pasandideh-Fard and J. Mostaghimi, Droplet Impact and Solidification in a Thermal Spray Process: Droplet-Substrate Interactions, *Thermal Spray: Practical Solutions for Engineering Problems*, C.C. Berndt, Ed., ASM International, 1996, p 637-646
30. V.V. Sobolev and J.M. Guilemany, Influence of Droplet Impact Angle on Droplet-Substrate Mechanical Interaction in Thermal Spraying, *Mater. Lett.*, Vol 33, 1998, p 315-319
31. O.G. Engel, Waterdrop Collisions with Solid Surfaces, *J. Res. Nat. Bur. Stand.*, Vol 54 (No. 5), 1955, p 281-298
32. S.S. Kutateladze, V.E. Nakoryakov, V.V. Sobolev, and I.R. Shreiber, Dynamics of Shock Waves in Liquid Containing Gas Bubbles, *J. Appl. Mech. Tech. Phys.*, (No. 5), 1974, p 67-71
33. V.G. Gasenko and V.V. Sobolev, Evolution of Finite Perturbations in Viscoelastic Relaxing Liquid with Gas Bubbles, *Comm. Acad. Sci. USSR Mech. Liq. Gas*, (No. 3), 1975, p 52-58
34. V.G. Gasenko and V.V. Sobolev, Pulsations of Gas Bubbles in Nonewtonian Liquid under Action of Sound Field, *Comm. Acad. Sci. USSR Mech. Liq. Gas*, (No. 2), 1974, p 129-135
35. V.V. Sobolev, On Propagation of Perturbations in Viscoelastic Gas-Liquid Medium, *Nonlinear Wave Processes in Two Phase Media, Inst. Thermophys.*, Sib. Br. Acad. Sci. USSR, Novosibirsk, 1977, p 45-53
36. D.T. Gawne, B.J. Griffiths, and G. Dong, Splat Morphology and Adhesion of Thermally Sprayed Coatings, *Thermal Spraying—Current Status and Future Trends*, A. Ohmoro, Ed., High Temperature Society of Japan, 1996, p 779-784
37. V.V. Sobolev, J.M. Guilemany, and J.A. Calero, Substrate-Coating Thermal Interaction during High Velocity Oxy-Fuel (HVOF) Spraying. Part 1. Heat Transfer Processes, *Mater. Sci. Technol.*, Vol 11 (No. 8), 1995, p 810-819
38. V.V. Sobolev, J.M. Guilemany, J.A. Calero, and F.J. Villuendas, Heat Transfer between WC-Co Coating and Aluminium Alloy Substrate during High Velocity Oxygen-Fuel (HVOF) Spraying, *J. Therm. Spray Technol.*, Vol 4 (No. 4), 1995, p 408-414
39. M. Vardelle, A. Vardelle, A.C. Leger, P. Fauchais, and D. Gobin, Influence of Particle Parameters at Impact on Splat Formation and Solidification in Plasma Spraying Processes, *J. Therm. Spray Technol.*, Vol 4 (No. 1), 1994, p 50-58

40. W. Kurz and D.J. Fischer, Fundamentals of Solidification, *Trans. Tech.*, Aedermannsdorf, 1984

41. V.V. Sobolev, Morphology of Splats of Thermally Sprayed Coatings, *Thermal Spray: Meeting the Challenges of the 21st Century*, C. Coddet, Ed., ASM International, 1998, p 507-510

42. A.C. Leger, M. Vardelle, A. Vardelle, P. Fauchais, S. Sampath, C.C. Berndt, and H. Herman, Plasma Sprayed Zirconia: Relationships between Particle Parameters, Splat Formation and Deposit Generation—Part 1: Impact and Solidification, *Thermal Spray: Practical Solutions for Engineering Problems*, C.C. Berndt, Ed., ASM International, 1996, p 623-628

43. A. Hasui, S. Kitahara, and T. Fukushima, On Relation between Properties of Coating and Spraying Angle in Plasma Jet Spraying, *Trans. Natl. Res. Inst. Met.*, Vol 12, 1970, p 9-20

44. R.C. Tucker and M.O. Price, The Effect of Angle of Deposition on the Properties of Selected Detonation Gun Deposits, *Proc. Int. Symp. Adv. Therm. Technol. Allied Depos. (ATTAC)*, Osaka, 1988, p 61-71

45. M.F. Smith, R.A. Neiser, and R.C. Dykhuizen, An Investigation of the Effects of Droplet Impact Angle in Thermal Spray Deposition, *Thermal Spray Indust. Applications*, C.C. Berndt and S. Sampath, Ed., ASM International, 1994, p 603-608

46. G. Montavon, C. Coddet, S. Sampath, H. Herman, and C.C. Berndt, Vacuum Plasma Spray Forming of Astroloy: An Investigation of Processing Parameters, *Thermal Spray Industrial Applications*, C.C. Berndt and S. Sampath, Ed., ASM International, 1994, p 469-475

47. V.V. Sobolev and J.M. Guilemany, Effect of Droplet Impact Angle on Flattening of Splat in Thermal Spraying, *Mater. Lett.*, Vol 32, 1997, p 197-201